3-1-1996

Studies of thin strained InAs, AlAs, and AlSb layers by spectroscopic ellipsometry

C. M. Herzinger
University of Nebraska-Lincoln

Paul G. Snyder
University of Nebraska-Lincoln, psnyder1@unl.edu

F. G. Celii
Texas Instruments, Central Research Lab, Dallas, Texas

Y.-C. Kao
Texas Instruments, Central Research Lab, Dallas, Texas

D. Chow
Hughes Research Laboratory, Malibu, California

See next page for additional authors

Studies of thin strained InAs, AlAs, and AlSb layers by spectroscopic ellipsometry

C. M. Herzinger[a] and P. G. Snyder
Center for Microelectronic and Optical Materials Research, and Department of Electrical Engineering University of Nebraska-Lincoln, Lincoln, Nebraska 68588-0511

F. G. Celii and Y.-C. Kao
Texas Instruments, Central Research Lab, Dallas, Texas 75265

D. Chow
Hughes Research Laboratory, Malibu, California 90265

B. Johs and J. A. Woollam
J.A. Woollam Co., Lincoln, Nebraska, 68588

(Received 28 November 1994; accepted for publication 13 November 1995)

The optical constants for thin layers of strained InAs, AlAs, and AlSb have been investigated by spectroscopic ellipsometry and multi-sample analyses. These materials are important for high-speed resonant tunneling diodes in the AlAs/InAs/$In_{0.53}Ga_{0.47}As$ and AlSb/InAs material systems. Understanding the optical properties for these thin layers is important for developing *in situ* growth control using spectroscopic ellipsometry. *Ex situ* room-temperature measurements were made on multiple samples. The resulting fitted optical constants are interpreted as apparent values because they are dependent on the fit model and sample structure. These apparent optical constants for very thin layers can be dependent on thickness and surrounding material, and are generally applicable only for layers found in a similar structural context. The critical point features of optical constants for the strained layers and for the thin unstrained cap layers were found to differ from bulk values, and three principle effects (strain, quantum confinement, and thin-barrier critical-point broadening) have been identified as responsible. Of these three, the broadening of the E_1 and $E_1+\Delta_1$ critical points for thin barrier material is the newest and most pronounced. This thin barrier effect is shown to be a separate effect from strain, and is also observable for the AlAs/GaAs system. [S0021-8979(96)04704-7]

I. INTRODUCTION

There is growing interest in double-barrier resonant-tunneling diodes (RTDs) with strained barriers because of the high-speed and large negative-differential-resistance effects which they exhibit. The AlAs/InAs/$In_{0.53}Ga_{0.47}As$ and AlSb/InAs material systems are of primary interest.[1–3] The first system uses strained AlAs barriers and a strained InAs well embedded in $In_{0.53}Ga_{0.47}As$ layers which are lattice matched to InP. In this system, the very large strain in the AlAs barriers can be compensated by the opposing strain in the InAs well. The second material system typically uses thick InAs buffer layers grown on GaAs substrates, and the strain in the AlSb barriers is lower but uncompensated when compared to the first system. However, regardless of the material system very accurate thickness control is required to produce devices with uniform and reproducible electrical properties.

Spectroscopic ellipsometry (SE) is a powerful, nondestructive tool for accurate thickness determination of thin layers[4] which can be used for both *ex situ* calibration of the growth process and for direct *in situ* growth control.[5,6] Ellipsometry is an indirect technique for thickness determinations because the measured data must be fit to a layered model which utilizes appropriate optical constants. For *in situ* growth control, these optical constants must of course be for the correct growth temperature; however, room-temperature *ex situ* measurements can provide insight into how the strained layer optical constants compare with the more easily determined bulk values. *Ex situ* variable angle spectroscopic ellipsometry (VASE) measurements can provide greater spectral detail and a higher signal-to-noise ratio than *in situ* measurements, thereby allowing the dominant effects which alter the bulk optical constants to be more easily identified. For these layers, both strain-induced and quantum-mechanical thickness effects are present. For each of the three materials, samples with single strained layers were examined with the primary focus on how the strained and bulk optical constants differ. Because of the mathematical correlation between optical constants and layer thickness in the fitting procedure, this requires a multi-sample approach where data from more than one sample are simultaneously analyzed to find thicknesses along with a common set of optical constants for the different samples.

Section II presents a discussion of the various possible interpretations of thickness for the very thin layers used in this work. Section III covers the basic terminology for discussing SE data fits. Section IV describes the data acquisition and modeling procedures used to determine optical constants from the strained InAs, AlAs, and AlSb layers measured for this work. The differences between these optical constants and bulk values are then discussed in terms of strain and thickness effects in Sec. V. Section VI comments on the con-

[a]Currently with J. A. Woollam Co., Inc.

sequences of this *ex situ* analysis for potential spectroscopic ellipsometry growth control schemes. Final conclusions are presented in Sec. VII.

II. IS THICKNESS A UNIQUELY DEFINED QUANTITY?

The very thin (<30 Å) strained layers considered here are composed of only several monolayers, and differences on the submonolayer level are important. In this case, the meaning of ''thickness'' is not exact and the appropriate definition depends on what property is being described and how it is measured. At least four possible thickness meanings need to be considered: ''true,'' ''electrical,'' ''optical,'' and ''nominal.'' Since the material is crystalline, a true thickness which is not an integral number of monolayers, say 4.3 monolayers, is best described as a 30:70 coverage mix of 4 and 5 monolayers. Except for specially prepared and destructively tested samples, this true thicknesses is unknown and can only be inferred from other measured values. For the case of a RTD, the electrical thicknesses are those values that best describe the device operation (fit the measured $I-V$ curves) using a good device physics model. For barriers, this thickness determines transmission probabilities for electron tunneling. In a similar way, the optical thickness is that value which best describes the ellipsometric model used to fit the measured data, but it incorporates information about different electronic states than the electrical value. Ellipsometry is typically more sensitive to the states related to the E_1 and $E_1+\Delta_1$ critical points (CPs) near the Λ point in the Brillouin zone. Without any direct feedback during growth, these measured thicknesses need to be related back to the nominal thickness which is determined by shutter (valve) timing and longer growth rate calibration runs. Maintaining precision and accuracy with an open loop timing system is difficult due to run-to-run variations in other growth parameters, especially substrate temperature and source fluxes.

Offsets between various meanings of thickness are not surprising and may be due to physical effects such as flux transients and interfacial effects, or they may simply represent built-in differences of definition. For electrical devices such as RTDs, ultimately uniformity and run-to-run reproducibility of the electrical thicknesses are most important; however, the electrical thicknesses can not be determined during growth, while optical thickness determinations are possible. Growth control does not require equivalence of the electrical with the optical thickness, only a one-to-one correspondence. With proper calibration, an ellipsometer used to form a closed feedback loop may be able to produce both precise and accurate electrical thicknesses on a run-to-run basis. In all cases, there should be a consistent one-to-one relation among the true, electrical, and optical thicknesses. The relationship with the nominal thickness, however, is likely to be more variable run to run. A closed-loop thickness control system using the optical thickness may be able to overcome the less stable relationship between true and nominal thicknesses.

III. EXPERIMENT AND VASE BASICS

Ellipsometry determines thicknesses and optical constants for layered samples by fitting the measured data to a parameterized model. The standard model for analyzing VASE data is a sequence of parallel layers with smooth interfaces and homogeneous optical constants, on a semi-infinite substrate.[7] Our fitting procedure is described more fully elsewhere,[8] but the basic terminology is given below. The standard ellipsometric parameters ψ and Δ are related to the complex ratio of reflection coefficients for light polarized parallel p and perpendicular s to the plane of incidence.[7] This ratio is defined as

$$\rho=\frac{R_p}{R_s}=\tan(\psi)e^{i\Delta}. \tag{1}$$

The electric-field reflection coefficient for p (s) polarized light is given by R_p (R_s). In addition to ψ and Δ, their standard deviations, $\sigma_\psi^{\text{expt}}$ and $\sigma_\Delta^{\text{expt}}$, are measured using multiple revolutions of the analyzer. (Multiple revolutions are used in any case to improve the signal-to-noise ratio for ψ and Δ.) A useful related quantity is the pseudodielectric function given by

$$\langle\epsilon\rangle=\langle\epsilon_1\rangle+i\langle\epsilon_2\rangle=\sin^2(\phi)\left[1+\left(\frac{1-\rho}{1+\rho}\right)^2\tan^2(\phi)\right], \tag{2}$$

which is less dependent on the angle of the incidence ϕ than are ψ and Δ. For layered samples, the pseudodielectric function can provide more insight than ψ and Δ can into what structure is present in the constituent layer optical constants. For a bare substrate, the pseudodielectric and intrinsic substrate dielectric functions are equivalent. The Levenberg–Marquardt algorithm[9] is used to fit the model parameters by minimizing the following weighted (biased) test function:[10]

$$\xi^2=\frac{1}{2N-M}\sum_{j=1}^{N}\left[\left(\frac{\psi_j^{\text{mod}}-\psi_j^{\text{expt}}}{\sigma_{\psi,j}^{\text{expt}}}\right)^2+\left(\frac{\Delta_j^{\text{mod}}-\Delta_j^{\text{expt}}}{\sigma_{\Delta,j}^{\text{expt}}}\right)^2\right]$$
$$=\frac{1}{2N-M}\chi^2. \tag{3}$$

The number of measured ψ and Δ pairs is N and the total number of real valued fit parameters is M. The figure of merit (FOM) we use to describe confidence in the ith fit parameter is given by

$$\text{FOM}_i=1.65\sqrt{C_{ii}}\xi. \tag{4}$$

This is the usual one-parameter, 90%, uncorrelated confidence limit[9] multiplied by our test function ξ, where C_{ii} is the ith diagonal element of the fit parameter covariance matrix.[8] In the case of a good fit with no systematic errors, ξ^2 tends toward a value of one and FOM_i reduces to the standard 90% confidence limit. This FOM combines information about the sharpness of the fit minimum (C_{ii}) with information about the overall quality of the fit. The FOM is primarily related to the combined measurement and fitting process. Using the FOM as direct quantitative information about the sample is only valid when $\sigma_\psi^{\text{expt}}$ and $\sigma_\Delta^{\text{expt}}$ are known to be accurate in magnitude, and when random (not systematic) measurement errors dominate the fit.[8]

TABLE I. Materials and nominal thicknesses for sample studied.

Sample	Material	Thickness (Å)	Cladding	t-cap (Å)	t-buffer (Å)	Grower	I.D.
1	InAs	20	$In_{0.53}Ga_{0.47}As$	60	2000	TI	7492
2	InAs	30	$In_{0.53}Ga_{0.47}As$	60	2000	TI	7495
3	AlAs	20	$In_{0.53}Ga_{0.47}As$	20	4000	TI	7441
4	AlAs	15	$In_{0.53}Ga_{0.47}As$	60	2000	TI	7502
5	AlAs	20	$In_{0.53}Ga_{0.47}As$	60	2000	TI	7504
6	AlAs	25	$In_{0.53}Ga_{0.47}As$	60	2000	TI	7505
7	AlAs	50	$In_{0.53}Ga_{0.47}As$	20	4000	TI	7434
8	AlAs	50	$In_{0.53}Ga_{0.47}As$	60	2000	TI	7503
9	AlSb	15	InAs	30	10 000	HRL	407
10	AlSb	25	InAs	30	10 000	HRL	408
11	AlSb	15	InAs	30	10 000	HRL	480
12	AlSb	25	InAs	30	10 000	HRL	482

IV. DATA ACQUISITION AND MODELING

For this investigation 12 samples, each containing a single, thin strained layer were used (Table I). Samples 1 and 2 were used to study InAs on $In_{0.53}Ga_{0.47}As$. The basic model structure used for fitting the ellipsometric data from these samples is shown in Fig. 1(a). The $In_{0.53}Ga_{0.47}As$ oxide optical constants were constructed using a published model for semiconductor oxide optical constants,[11] and interpolated parameters between binary endpoints. The nominal thicknesses for the InAs samples, and for the other 10 samples, are given in Table I. The basic structure for the AlAs on $In_{0.53}Ga_{0.47}As$ samples 3–8 is shown in Fig. 1(b). For analysis, the AlAs samples were broken into two groups with t-AlAs <30 Å (samples 3–6) and with t-AlAs ~ 50 Å (samples 7 and 8). The final group of four AlSb samples had the nominal structure shown in Fig. 1(c).

Before presenting the detailed analysis of these four sample groupings, several general concepts involved need to be covered.

(1) The primary goal is to find optical constants for the strained layers; however, this is very difficult to do because there are overlayers (oxides and semiconductor caps) present, the strained layers are very thin, and only nominal thicknesses are known. Acquisition at variable angles can help in determining thicknesses and optical constants simultaneously,[12] but this requires the special conditions of low absorption, t_{layer} at least on the order of λ_{probe}, and a substrate with very different optical constants. For these strained samples which are optically thin and have relatively low optical contrast with the substrate and cap, variable angle data are primarily useful as independent measurements to reduce experimental noise at each wavelength. Furthermore, the thin cap layers may not be well represented by bulk optical constants as has been observed for thin GaAs caps on AlAs.[13] Therefore, more than one set of optical constants may need to be determined. (For *ex situ* ellipsometry, cap layers are needed to protect the layers of interest from oxidation.)

(a)

In(0.53)Ga(0.47)As Oxide	t-ox
In(0.53)Ga(0.47)As	t-cap
InAs	t-InAs
In(0.53)Ga(0.47)As	t-buffer
InP	substrate

(b)

In(0.53)Ga(0.47)As Oxide	t-ox
In(0.53)Ga(0.47)As	t-cap
AlAs	t-AlAs
In(0.53)Ga(0.47)As	t-buffer
InP	substrate

(c)

InAs Oxide	t-ox
InAs	t-cap
AlSb	t-AlSb
InAs	t-buffer
GaAs	substrate

FIG. 1. Layered models used to analyze ellipsometric data for samples (a) 1 and 2 (b) 3–8, and (c) 9–12.

(2) Two sets of optical constants and layers thicknesses cannot be determined from data acquired from a single sample; therefore, for this work, multi-sample analyses were used. For each of the four groupings already described, the data from the samples were simultaneously analyzed to determine layers thicknesses and a common set of optical constants for the strained layers. A multi-sample analysis can be used to reduce correlation between optical constants and layer thicknesses, but is most powerful when the layer of interest creates its own well-defined interference pattern.[12,13] For the optically thin strained layers considered here, the multi-sample analysis will not determine all the model parameters uniquely; however, it will reduce the correlation to a manageable level, such that a few simple approximations will allow the analysis to proceed.

(3) The optical constants we determine for the thin layers are best interpreted as apparent optical constants. The term apparent is used to imply that the optical constants may be dependent on thickness and surrounding material, and may therefore be applicable only for layers found in the same context. In fact, there is no obvious reason to assume that optical constants should be the same for the slightly different thicknesses considered here, but that assumption is made to permit multi-sample analyses. Thus, the optical constants are average values for the available measured thicknesses. Furthermore, the data fitting procedure assumes that each layer

can be described as a homogeneous layer with perfect interfaces. In fact, for the very thin layers considered here, the wave functions for the involved optical transitions can easily extend outside the model layer thickness. Therefore, the optical constants are context sensitive because they are a function of the surrounding material and surrounding layer thicknesses (e.g., a 50 Å layer of GaAs can have very different apparent optical constants depending on whether it is surrounded by AlAs or GaAs). For the simple, purely optical models used for ellipsometric analysis, this context sensitivity is not explicitly modeled, but it is incorporated into the resulting fitted optical constants. The final optical constants are apparent values because they are constrained to fit the measured data within the modeling procedure (homogenous within a bounded layer) and they represent an average over thickness and contexts (surrounding layers).

(4) Mathematical correlation between layer thicknesses and optical constants is reduced but not eliminated by a multi-sample analysis; therefore, it is necessary to ''fix'' one of the strained layer thicknesses in each group. One of the samples within a group will be considered to have $t_{\text{strained}}=t_{\text{nom}}$. This defines the optical and nominal thicknesses for one of the samples to be identical. Although somewhat arbitrary, it is reasonable since we have already noted in Sec. II that very thin layers may not have a unique definition of thickness. By fitting the thicknesses for the other samples in the group, the proper relative thicknesses will be determined.

(5) To simplify the analysis further, oscillator ensembles were used to describe the cap and strained-layer optical constants as an intermediate procedure to determine layer thicknesses.[13] Oscillator ensembles have been used to model semiconductor critical point (CP) structures for energies above the direct band gap.[14–16] This modeling technique employs oscillators at the major critical points, with extra ''fictitious'' oscillators to fill in the absorption between critical points,

$$\epsilon(\hbar\omega)=\epsilon_1^{\text{offset}}+\sum_j \frac{A_j}{E_j^2-(\hbar\omega)^2-iB_j\hbar\omega}. \tag{5}$$

Bulk optical constants for the cap and strained layer materials were modeled using oscillators as in Eq. (5). Then, the energy and broadening parameters, but not the amplitudes, of these models were allowed to vary while fitting the layer thicknesses. This provided a method to allow the optical constants to vary from bulk values into the thin cap and thin strained layer values while fitting a very limited number of parameters. Because the amplitudes were not allowed to vary, the overall absorption strength of a layer was preserved while allowing it to be redistributed. Oscillators cannot describe the sharp change in absorption at the lowest-energy direct gaps, however, and an oscillator ensemble is usually a very poor model below and just above such a CP. (In Ref. 16 a variable phase factor was included, which improved the ability to model M_0 transitions.) However, for this work oscillators were still used as an intermediate step for both AlAs and AlSb which have direct gaps in the region of interest. The oscillators were satisfactory because the AlAs and AlSb layers were thin, producing no interference pattern and there is limited sensitivity to the absolute level of absorption around the band gap. Bulk InAs and $In_{0.53}Ga_{0.47}As$ optical constants were modeled quite well by oscillators for this work.

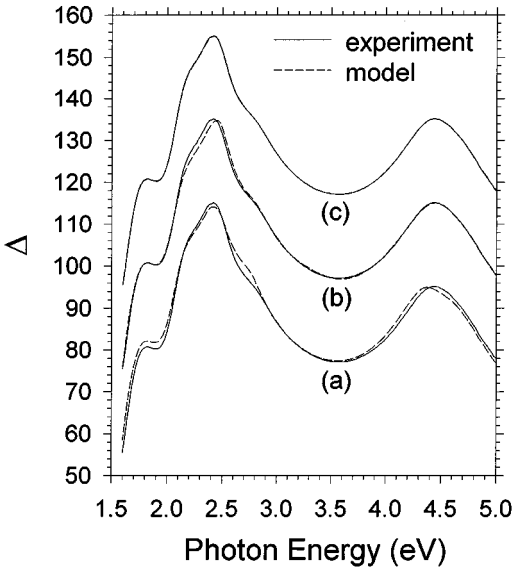

FIG. 2. Data fits at 76° angle of incidence for strained InAs sample 2 using successively refined models. (Table II summarizes thickness results for multi-sample analyses of samples 1 and 2.) (a) Assuming bulk optical constants and fitting only thicknesses yields a poor fit. Allowing the InAs oscillator parameters to vary improves the fit [(b), shown offset by 20°]. Final fit was obtained by fitting strained InAs dielectric constants at each wavelength [(c), shown offset by 40°].

(6) Within a group (InAs, AlAs, or AlSb), the samples were measured consecutively and in the same manner with respect to integration time, monochromator bandpass, and ambient light conditions. This was done for the multi-sample analysis to keep the data from each sample correctly weighted with respect to the other samples within that group. The standard ellipsometric parameters, ψ and Δ, were measured spectroscopically covering the bulk material E_1 and E_2 (CP) regions for both cladding and strained layers.

A. InAs

The InAs sample group consisted of samples 1 and 2. These samples were measured and analyzed in the spectral range from 1.6 to 5.0 eV for incident angles of 74° and 76°. Three successive analysis procedures were performed using models with increasing degrees of freedom. The resulting fits of Δ at one incident angle for sample 2 are shown in Fig. 2. Table II summarizes the fit quality and thickness results for both samples. The first modeling procedure assumed that all layers had optical constants appropriate for bulk material, and that only the layer thicknesses needed to be fit. This approach produced poor fits [Fig. 2(a)] with thicknesses quite different from nominal.

For the second analysis, the InAs optical constants were modeled using an oscillator ensemble [Eq. (5)] with starting parameters obtained by fitting to bulk InAs values. The strained InAs layer thickness for sample 2 was fixed at 30 Å forcing the nominal and optical thicknesses to be the same. Furthermore, because of anticipated correlation between

TABLE II. Fitting results for strained InAs samples. Thicknesses in Å, FOM [Eq. (4)] in parentheses. (a)–(c) correspond to model fits in Fig. 2.

Sample	Fit parameter	Nominal thickness	(a) InAs—bulk cap—bulk	(b) InAs—fit, osc. cap—bulk	(c) InAs—fit, table cap—bulk
1	t-ox	0	19.2 (0.20)	19.2 (0.13)	19.3 (0.02)
	t-cap	60	75.2 (3.5)	45.9 (1.8)	46.3 (0.4)
	t-InAs	20	39.0 (1.9)	21.5 (0.5)	21.1 (0.1)
	t-buffer	2000	2211.0 (8.3)	2259.2 (3.8)	2257.6 (1.0)
2	t-ox	0	17.3 (0.18)	18.0 (0.13)	18.0 (0.02)
	t-cap	60	72.8 (2.2)	50	50.0 (0.2)
	t-InAs	30	56.4 (1.8)	30	30.0 (0.1)
	t-buffer	2000	2266.1 (6.9)	2315.1 (2.8)	2266.1 (6.9)
		$\chi^2/2N$	1052.4	219.2	15.5

thicknesses and optical constants for a fit involving only two samples, the cap thickness was also fixed. It was fixed at 50 Å allowing for 10 Å of the nominal thickness to be consumed by oxidation. The broadening and energies (10 parameters) for the InAs oscillators were fit along with six layer thicknesses. The fits improved [Fig. 2(b)], especially in the E_2 CP region at 4.4 eV. Attempts at fitting the cap optical constants as well as the InAs optical constants did not produce better fits in the final analysis. This is due in part to the overlap of the CP structures for InAs and $In_{0.53}Ga_{0.47}As$. This is discussed further in Sec. V.

The final analysis for these samples allowed the InAs optical constants at all measured wavelengths to be simultaneously fit with five layer thicknesses. For sample 2, the oxide, cap, and InAs thicknesses from the previous procedure were used as fixed values. Once the fit minimization was completed, the wavelength-by-wavelength optical constant table for the strained InAs was saved and fixed in the model. Finally, the stability of the fits using these optical constants was demonstrated by resetting the layer thicknesses to their nominal values and refitting. The results of this thickness-only fit (which are identical to those before the refit) are given in the last column of Table II. The final fit is very good [Fig. 2(c)] and therefore the assumed cap thickness for sample 2 was not a severe constraint. In actuality, what has happened is that the correlation between cap thickness and strained layer optical constants has been transferred into the solved optical constants. Thus, if the actual cap thickness should have been 60 Å, then future fits using these optical constants will produce cap thicknesses approximately 10 Å too small. The final apparent strained InAs optical constants are compared with bulk values in Fig. 3. Interpretation of these results is given in Sec. V.

Table II includes both thicknesses and confidence FOMs for the three data modeling procedures. As discussed in Sec. III, the FOM [Eq. (4)] we use to describe confidence in a fit parameter is best used in a relative sense, not in absolute magnitude. (For this work, the assumptions needed to assign independent significance to the FOM magnitude are not clearly met.) The FOM magnitudes for the oxide thicknesses seem unphysically small, but they should only be compared with other FOMs from a particular fit or with FOMs for oxide thicknesses from different analyses of the same measured data. For instance, it is quite general to say that the oxide layer thickness is more precisely determined than is the buffer layer thickness. It is also general to note that the oxide and strained layer thicknesses are more precisely determined than are the cap layer thicknesses. This is because the cap and buffer layers are the same material and the fitting algorithm has less sensitivity determining the relative reflection contributions from these two layers due to their nearly identical optical properties. Similar observations are valid for all four sample groupings.

B. AlAs

The AlAs samples are broken into two groups: the thin group (samples 3–6, t-AlAs <30 Å) and the thick group (samples 7 and 8, t-AlAs ~ 50 Å). The nominal 50 Å thicknesses for the thick group are above the critical limit for strain relaxation as determined by laser light scattering,[17] so these layers are at least partially relaxed. The samples from both groups were measured from 1.5 to 5.0 eV at incident angles of 74° and 76°. For the analysis results presented in Table III, only data from 2.4 to 5.0 eV were used. The resulting Δ fits for one sample (5) are shown in Fig. 4 using the

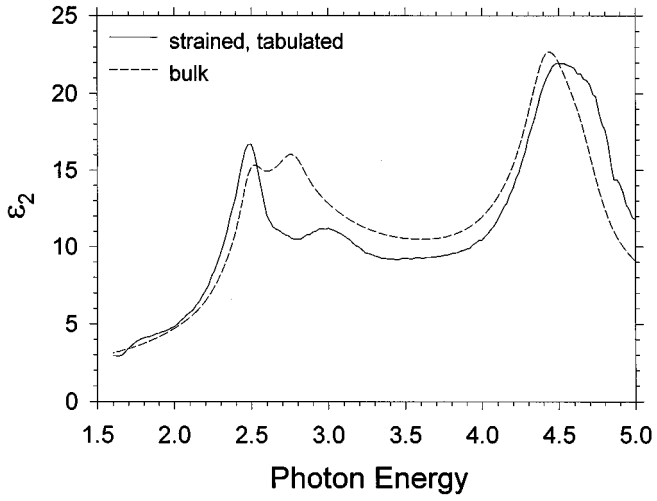

FIG. 3. Comparison of bulk InAs and apparent thin strained InAs dielectric functions (imaginary part).

TABLE III. Fitting results for thinnest strained AlAs samples. Thicknesses in Å, FOM [Eq. (4)] in parentheses. (a)–(c) correspond to model fits in Fig. 4.

Sample	Fit parameter	Nominal thickness	(a) InAs—bulk cap—bulk	(b) InAs—fit, osc. cap—bulk	(c) InAs—fit, table cap—bulk	(d) AlAs—fit, table cap—previous fit
3	t-ox	0	20.9 (0.31)	20.6 (0.18)	19.8 (0.10)	19.9 (0.03)
	t-cap	20	64.8 (1.4)	18.3 (1.2)	29.7 (1.6)	29.7 (0.13)
	t-AlAs	20	23.7 (0.50)	27.4 (0.28)	20.4 (0.29)	20.4 (0.05)
	t-buffer	4000	4186.0	4186.0	4186.0	4169.5 (5.6)
4	t-ox	0	16.5 (0.32)	16.6 (0.12)	16.4 (0.14)	16.4 (0.03)
	t-cap	60	116.7 (2.6)	72.2 (1.3)	72.9 (2.7)	72.4 (0.2)
	t-AlAs	15	17.2 (0.83)	16.2 (0.12)	15.4 (0.15)	15.4 (0.05)
	t-buffer	2000	2217.0	2217.0	2217.0	2218.3 (0.7)
5	t-ox	0	17.4 (0.33)	16.2 (0.12)	17.1 (0.14)	17.0 (0.03)
	t-cap	60	109.3 (2.1)	58.4 (1.2)	70.3 (2.6)	70.8 (0.2)
	t-AlAs	20	21.9 (0.82)	20	20	20.2 (0.06)
	t-buffer	2000	2175.3	2175.3	2175.3	2172.5 (0.7)
6	t-ox	0	15.3 (0.33)	15.1 (0.14)	14.9 (0.14)	14.8 (0.03)
	t-cap	60	112.5 (1.7)	66.7 (1.1)	75.1 (2.2)	76.7 (0.17)
	t-AlAs	25	27.1 (0.82)	31.3 (0.42)	24.4 (0.16)	25.3 (0.06)
	t-buffer	2000	2181.8	2181.8	2181.8	2180.0 (0.7)
		$\chi^2/2N$	2393.2	280.0	41.9	24.2

same format as Fig. 2. (Fits for the thick AlAs group are similar but not shown.) The first procedure for the thin AlAs group assumed bulk optical constants for all layers and fit only 12 thicknesses. The buffer layer thicknesses were estimated from a preliminary analysis including the data below 2.4 eV. The resulting poor fit quality is shown in Fig. 4(a). Note the E_1 CP structure from AlAs is present in the model but not in the data.

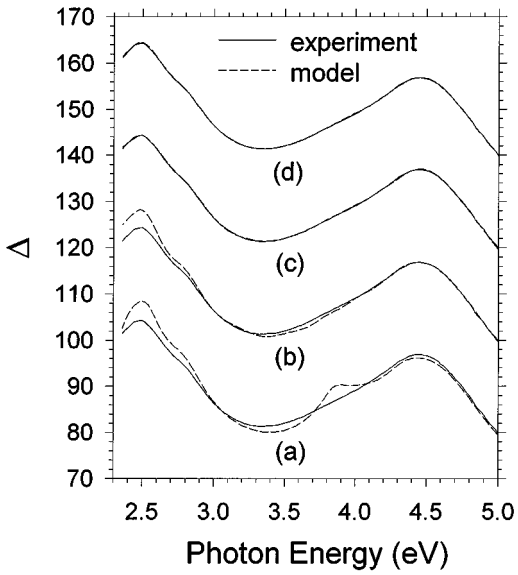

FIG. 4. Data fits at 76° angle of incidence for AlAs sample 5. (Table III summarizes thickness results for multi-sample analyses of samples 3–6.) (a) Assuming bulk optical constants and fitting only thicknesses yields a poor fit. Allowing AlAs oscillator parameters to vary improves the fit [(b), shown offset by 20°]. Allowing some of the cap $In_{0.53}Ga_{0.47}As$ oscillator parameters to vary improves the fit further [(c), shown offset by 40°]. Using previously fit cap optical constants and fitting strained AlAs dielectric values at each wavelength yields the final, best fit [(d), shown offset by 60°].

Next, the AlAs bulk optical constants were replaced by an oscillator group that closely fit the bulk values above 3.0 eV. The spectral analysis region was limited because the oscillators cannot adequately model a semiconductor below the direct band gap. However, the E_1 CP structure for the $In_{0.53}Ga_{0.47}As$ needed to be included, so a compromise range, 2.4–5.0 eV, was used. The AlAs thickness for sample 5 was fixed at the nominal 20 Å value. The remaining oxide, cap, and AlAs thicknesses (11 parameters) were fit along with the AlAs broadenings and energies (10 parameters). The fit [Fig. 4(b)] improved, but problems around the $In_{0.53}Ga_{0.47}As$ E_1 CP remained.

In the next fit, the cap optical constants (oscillator parameters) were also allowed to vary. In fact, because the samples had different nominal cap thicknesses, two different cap optical spectra were fit for sample 3 and for samples 4–6. These cap optical constants were not allowed to be totally independent, however. Only the E_1 and $E_1+\Delta_1$ CP oscillator parameters were fit separately. The parameters constituting the E_2 CP structure were coupled together for the cap layers, and these parameters were also fit. The much improved fit is shown in Fig. 4(c). The resulting cap optical constants are shown compared with bulk $In_{0.53}Ga_{0.47}As$ in Fig. 5. Note the E_2 structure is quite similar to bulk, but that the E_1 CP structure is quite different especially for the thinner 20 Å nominal cap of sample 3.

These new cap optical constants were then saved and fixed into the model for the final determination of the AlAs optical constants at all the measured wavelengths. The oxide, cap, and AlAs thickness for sample 5 were fixed at their values from the previous fit. Then the remaining samples' oxide, cap, and AlAs thicknesses were fit simultaneously with the AlAs optical constants. Next, the oxide, cap, and AlAs thicknesses for all four samples were fixed and the spectral range was increased from 1.5 to 5.0 eV. For this new

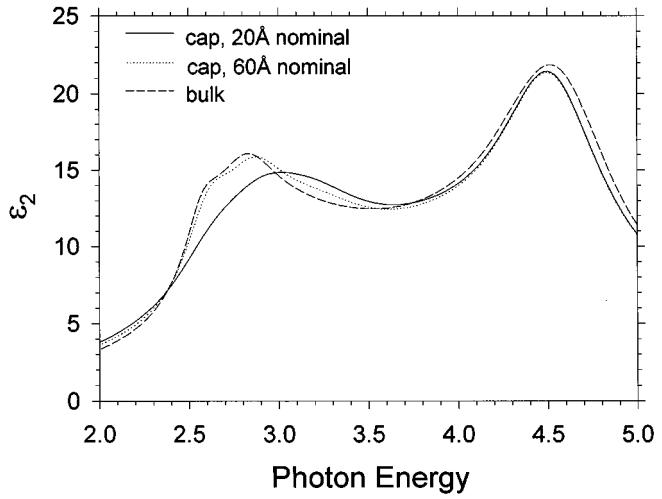

FIG. 5. Comparison of bulk $In_{0.53}Ga_{0.47}As$ and apparent cap $In_{0.53}Ga_{0.47}As$ dielectric functions used to model samples 3–6.

range, the AlAs optical constants and buffer layer thicknesses were fit. As with the final InAs analysis, these optical constants were saved, fixed in the model, and the thicknesses refit after being set to their nominal values. The results of this thickness-only fit, and those of the previous fits, are summarized in Table III. The final apparent strained AlAs optical constants from the thin AlAs group are compared with bulk values and with the results of the thick AlAs group in Fig. 6. Note that the imaginary part of the dielectric constant goes to zero (ϵ_2 was not allowed to be negative during fitting) and that an oscillator model could not describe such a function over the full measurement range.

For the thicker AlAs group, bulk AlAs optical constants also gave unsatisfactory fits; however, a complete analysis was not possible because only two samples were available. Therefore, to simplify the analysis, cap optical constants were taken from samples from the thin AlAs group with the same nominal cap thickness. Thus sample 7 used the cap results from sample 3, and sample 8 used values from

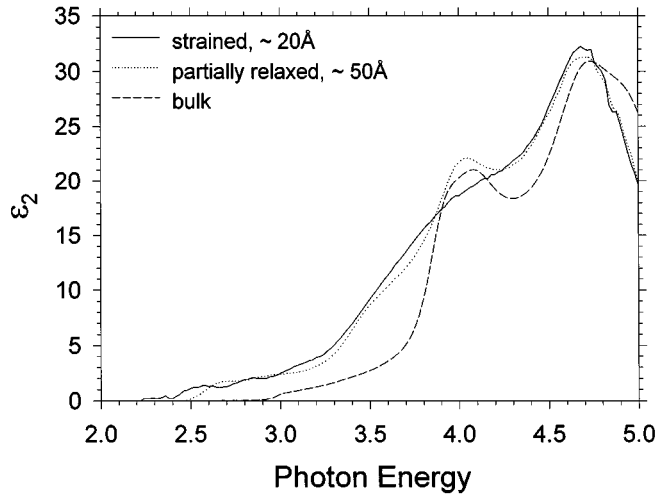

FIG. 6. Comparison of bulk tabulated AlAs, thinnest (~20 Å) strained AlAs, and nominally 50 Å strained AlAs dielectric functions (imaginary part).

TABLE IV. Fitting results for thicker AlAs samples. Thicknesses in Å, FOM [Eq. (4)] in parentheses.

Sample	Fit parameter	Nominal	AlAs—fit, osc. cap—previous fit	AlAs—fit, table cap—previous fit
7	t-ox	0	20.1 (0.24)	20.2 (0.07)
	t-cap	20	46.6 (0.5)	46.8 (0.1)
	t-AlAs	50	58.1 (0.29)	59.0 (0.10)
	t-buffer	4000	4186	4069.5 (7.5)
8	t-ox	0	15.6 (0.18)	15.5 (0.05)
	t-cap	60	87.6 (2.2)	87.7 (0.2)
	t-AlAs	50	46.2 (1.8)	46.5 (0.09)
	t-buffer	2000	2217	2189.0 (1.3)
		$\chi^2/2N$	1052.4	219.2

samples 4–6. The remaining analysis exactly paralleled that of the thin AlAs group. The thickness fit results are given in Table IV and the final optical constants are shown in Fig. 6.

C. AlSb

The AlSb group comprised four samples, 9–12. These samples were measured from 1.5 to 5.0 eV. However, like the thin AlAs group, a reduced range (2.45–4.7 eV) was used for the primary analysis. The optical constants were extended over the full measured range in the final step. In other respects the analysis procedure was exactly the same as for the thin AlAs group. For sample 12, the fit results for each of the model refinements is shown in Fig. 7(a)–7(d). Table V lists the fit parameters for samples 9–12.

Sample 12 had its AlSb thickness fixed at the nominal value. Two different cap optical constants were also employed in the same manner: Allow different E_1 structures,

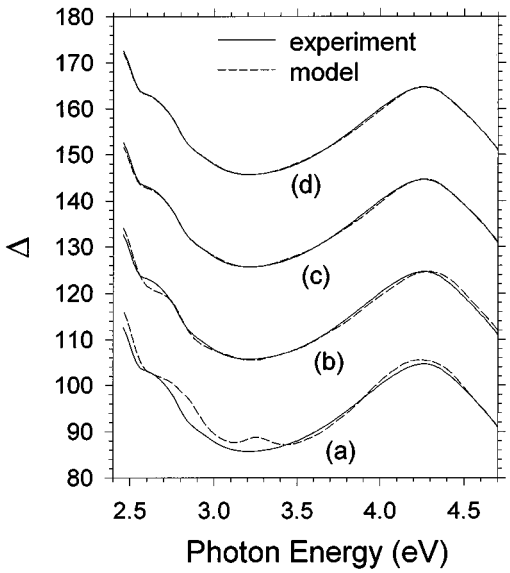

FIG. 7. Data fits at 75° incidence for AlSb sample 12. (Table V summarizes thickness results for multi-sample analyses of samples 9–12.) (a) Assuming bulk optical constants and fitting thicknesses only yields a poor fit. Allowing AlSb oscillator parameters to vary improves the fit [(b), shown offset by 20°]. Allowing some of the cap InAs oscillator parameters to vary improves the fit further [(c), shown offset by 40°]. Final fit was obtained using previously determined cap optical constants and fitting strained AlSb dielectric constants at each wavelength [(d), shown offset by 60°].

TABLE V. Fitting results for strained AlSb samples. Thicknesses in Å, FOM [Eq. (4)] in parentheses. (a)–(d) correspond to model fits in Fig. 7.

Sample	Fit parameter	Nominal thickness	(a) InAs—bulk cap—bulk	(b) InAs—fit, osc. cap—bulk	(c) InAs—fit, table cap—bulk	(d) AlSb—fit, table cap—previous fit
9	t-ox	0	13.2 (0.91)	14.0 (0.53)	14.1 (0.23)	14.2 (0.07)
	t-cap	30	0 (5.5)	18.9 (5.3)	18.1 (1.3)	18.0 (0.2)
	t-AlSb	15	9.1 (0.85)	14.9 (0.40)	14.1 (0.28)	14.5 (0.10)
10	t-ox	0	11.8 (0.70)	12.8 (0.69)	12.7 (0.29)	12.8 (0.05)
	t-cap	30	0 (3.2)	11.4 (5.0)	18.5 (1.7)	18.5 (0.15)
	t-AlSb	25	12.3 (0.62)	20.8 (0.40)	24.1 (0.66)	24.3 (0.09)
11	t-ox	0	13.5 (0.85)	13.9 (0.51)	13.8 (0.29)	14.5 (0.07)
	t-cap	30	0 (4.7)	27.7 (5.2)	24.7 (1.6)	24.2 (0.2)
	t-AlSb	15	9.8 (0.71)	15.6 (0.40)	12.6 (0.35)	14.3 (0.10)
12	t-ox	0	13.3 (0.87)	13.7 (0.75)	14.0 (0.39)	14.0 (0.06)
	t-cap	30	0 (3.2)	25.3 (4.9)	33.8 (1.7)	33.0 (0.2)
	t-AlSb	25	15.8 (0.78)	25	25	25.0 (0.11)
		$x^2/2N$	4010.4	410.2	25.1	20.1

couple the E_2 structures, and fit both. (The decision to employ different cap optical constants was arrived at because the cap thicknesses for samples 9 and 10 consistently fit to thinner values than for samples 11 and 12, even though they all had the same nominal 30 Å cap. If in fact the cap thicknesses of samples 11–12 had solved out to be the same as for samples 9–10, then the duplicate samples would have provided no additional information.) The two sets of cap optical constants are shown compared to bulk values in Fig. 8. The final apparent strained AlSb optical constants are shown compared to bulk in Fig. 9.

For all the optical constant spectra just described, a level of correlation between thicknesses and other layer optical constants is probably present due to a lack of sensitivity even with multi-sample analyses. However, this correlation is primarily related to the overall amplitudes; the location and shape of CP structures in the resulting optical constants are more adequately determined.

V. INTERPRETATION OF RESULTS

The thin cap and strained layer optical constants presented in the previous section can be explained qualitatively by three primary effects: strain, confinement-induced energy increases, and isolated thin-barrier CP broadening. The strained layer in each of these samples is under a (001) biaxial strain due to the lattice mismatch. Biaxial strain can produce both hydrostatic shifts and increased splitting of CP structures. Confinement induced energy increases are well known for both E_0 and E_1 CPs in quantum-well (QW) structures.[18,19] In this work, we noted energy blue shifts of the E_1 structure for some of the cap layers which are similar to those noted for GaAs caps on thick AlAs layers.[13] The most dramatic effect we observe is the almost complete washout of the E_1 CP structures for isolated thin AlAs and AlSb barrier layers. We attribute this primarily to a leakage of wave functions from the barrier layers into the surrounding material, not strain effects. This leakage would reduce

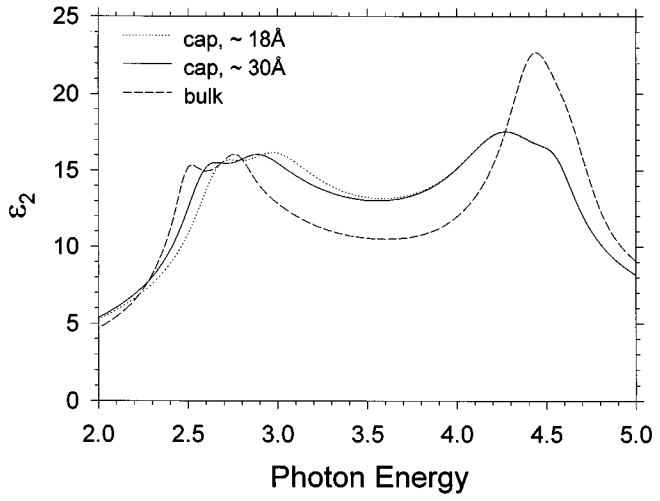

FIG. 8. Comparison of bulk InAs and apparent cap InAs dielectric functions used to model samples 9–12.

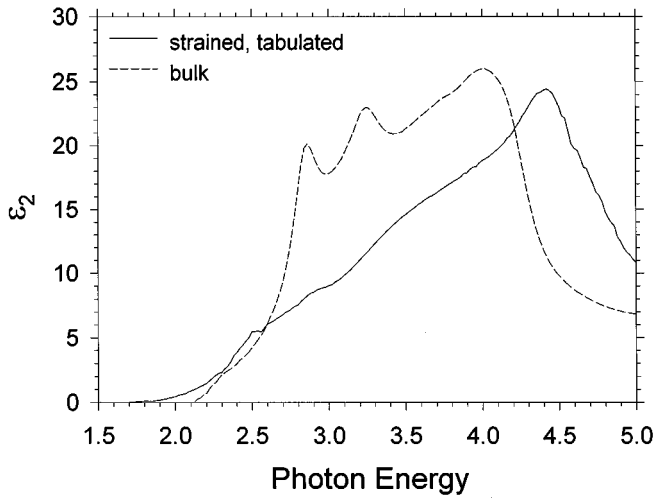

FIG. 9. Comparison of bulk AlSb and apparent thin strained AlSb dielectric functions (imaginary part).

TABLE VI. Parameters used for calculating strain model energy shifts.

Quantity	$InAs/In_{0.53}Ga_{0.47}As$	$AlAs/In_{0.53}Ga_{0.47}As$	AlSb/InAs
ϵ	−0.0313	+0.0369	−0.0127
c_{12}/c_{11}	0.5437[a]	0.4267[a]	0.4956[a]
α	−6.0 eV[a]	−9.8 eV[b]	−5.9 eV[a]
β	−1.8 eV[a]	−1.70eV[b]	−1.35eV[a]
E_1	−4.3 eV[c]	−4.3 eV[c]	−4.3 eV[c]
D_3^3	+3.45eV[c]	+3.45eV[c]	+3.45eV[c]
Δ_1	0.25eV[d]	0.20eV[d]	0.43eV[d]

[a]Reference 22.
[b]Taken from the GaAs values in Ref. 22.
[c]The required deformation potentials have been collected for only a few binaries, GaAs being the closest. These values were taken for GaAs from Ref. 23.
[d]Reference 24.

TABLE VII. Calculated and experimentally determined CP energy shifts.

Material	Critical point	Calc.	Expt.
InAs	$E_{0,hh}(\epsilon)-E_0(\epsilon=0)$	+0.05	⋯
	$E_1(\epsilon)-E_1(\epsilon=0)$	+0.03	−0.00
	$E_1\Delta_1(\epsilon)-E_1\Delta_1(\epsilon=0)$	+0.22	+0.18
AlAs (∼50 Å)	$E_{0,hh}(\epsilon)-E_0(\epsilon=0)$	−0.30	⋯
	$E_1(\epsilon)-E_1(\epsilon=0)$	−0.30	−0.39
	$E_1\Delta_1(\epsilon)-E_1\Delta_1(\epsilon=0)$	−0.06	−0.11
AlSb	$E_{0,hh}(\epsilon)-E_0(\epsilon=0)$	+0.04	⋯
	$E_1(\epsilon)-E_1(\epsilon=0)$	+0.04	⋯
	$E_1\Delta_1(\epsilon)-E_1\Delta_1(\epsilon=0)$	+0.07	⋯

state lifetimes and increase CP broadenings. The E_1 CP structure may be particularly susceptible to this kind of broadening due to its believed excitonic nature.[20,21]

Quantitative estimates for strain effects can be made using a perturbation analysis developed for E_0 and E_1 CPs under biaxial (001) strain by Pollak.[21,23] This approach has been used by Pickering *et al.* to explain strain induced increases (observed by SE) in the E_1, $E_1+\Delta_1$ splitting for $In_xGa_{1-x}As$ layers on GaAs,[25] and Si_xGe_{1-x} layers on Si.[26–28] The perturbation approximation may be less valid here due to the very large strain for these material systems, but the calculation can give some insight into the direction and relative magnitudes expected for the energy shifts. Strain should primarily change the band structure and thus the CP energies, but it should not significantly affect the CP broadening. Also, the calculations should be independent of thickness, provided that the layer is fully strained. Neglecting the excitonic-induced splitting, theoretical strain-induced energy shifts can be calculated using the following equations:[21,23]

$$E_{0,\mathrm{hh}}(\epsilon)-E_0(\epsilon=0)=2\alpha\left(1-\frac{c_{12}}{c_{11}}\right)\epsilon+\beta\left(1+2\frac{c_{12}}{c_{11}}\right)\epsilon, \quad (6)$$

$$E_1(\epsilon)-E_1(\epsilon=0)=\frac{\Delta_1}{2}+E_H-\frac{1}{2}\left(\Delta_1^2+4E_S^2\right)^{1/2} \quad (7)$$

$$E_1\Delta_1(\epsilon)-E_1\Delta_1(\epsilon=0)=\frac{-\Delta_1}{2}+E_H+\frac{1}{2}\left(\Delta_1^2+4E_S^2\right)^{1/2}, \quad (8)$$

where

$$E_H=2E_1\left(1-\frac{c_{12}}{c_{11}}\right)\epsilon, \quad E_S=\left(\frac{2}{3}\right)^{1/2}D_3^3\left(1+2\frac{c_{12}}{c_{11}}\right)\epsilon. \quad (9)$$

The biaxial strain is $\epsilon=(a_\epsilon-a_0)/a_0$, where a_0 and a_ϵ are the in-plane lattice constants for the material when unstrained and strained, respectively. The elastic constants for the material are c_{12} and c_{11}. The remaining terms in Eq. (6), α and β, are deformation potentials for the lowest Γ point transitions for hydrostatic and uniaxial (001) strain. The interband (E_1) and intraband (D_3^3) deformation potentials in Eq. (9) are for Λ_3–Λ_1 transitions. Table VI summarizes the deformation potentials and elastic constants used for the materials considered here. In principle, similar calculations could be performed for the E_2 CPs; however, our interest lies primarily in the E_1 CP region which is most useful for growth control schemes.

Calculations of confinement effects in QWs have been performed by others; however, we do not know of a simple method to calculate confinement induced shifts for cap layers. One complication is that half of the confinement is created by the oxide and vacuum levels and another problem is the imperfect oxide–cap interface which may be the source of some of the apparent broadening effects observed. We have made no quantitative calculations of cap energy shifts, but we expect and observe the general trend that thinner caps yield greater blue shifts in the extracted optical constants. We believe the washout of the E_1 CP structure for isolated barriers is a recent observation.[13] A similar broadening of AlAs E_1 structure was mentioned for thin barrier layers in a GaAs–AlAs superlattice structure.[29] We know of no quantitative calculations for this effect. This calculation is likely to be more complicated than a QW confinement problem because the decrease in state lifetimes within the barrier will involve coupling to a continuum of states in the surrounding material.

Examining the strained InAs results (Fig. 3), one first notes the increased splitting of the E_1 and $E_1+\Delta_1$ CPs. Strain-induced splitting has also been observed for strained $In_xGa_{1-x}As$ ($x<0.25$) on GaAs.[25] The energy shifts relative to bulk optical constants were determined by fitting the second derivative of the dielectric functions to the standard oscillator model with phase factor.[30] These shifts, along with calculated values using Eqs. (6)–(8), are given in Table VII. Note that calculated shifts for E_0 are also given, but that quantitative experimental results were not determined. For InAs, the E_0 CP is well outside our measurable spectral range. The calculated and experimentally determined shifts for the E_1 CPs are in good qualitative agreement, as in Refs. 25–28. For E_1, the hydrostatic and uniaxial components of the strain effect have opposite signs and compensate each other predicting a small energy change as is observed experimentally. For $E_1+\Delta_1$, the two components are calculated to be additive, creating a larger shift and increased splitting which are both confirmed experimentally. The cap layers for the InAs samples were treated as bulklike for the analyses presented in Sec. IV, and fits allowing the cap optical constants to vary did not produce better results. The explanation and justification for using bulklike $In_{0.53}Ga_{0.47}As$ cap optical

constants and for not including a confinement energy shift for the E_1 CPs are that the E_1 energies for InAs and $In_{0.53}Ga_{0.47}As$ nearly overlap. (InAs embedded in $In_{0.53}Ga_{0.47}As$ is definitely a QW for the Γ point.) In fact, after the strain is included, the InAs E_1 and $E_1+\Delta_1$ CPs may bracket the $In_{0.53}Ga_{0.47}As$ CP energies. Whether the InAs valence or conduction bands at Λ are confined in the InAs is dependent on the exact band alignment, but clearly both states can not be strongly confined. One tentative explanation for the apparently large change in broadening for the strained InAs $E_1+\Delta_1$ CP is that it is partially unconfined and is exhibiting the behavior of an isolated barrier while the E_1 CP is weakly confined maintaining broadening similar to bulk and no obvious confinement shift. We cannot derive great detail about the CPs because the overlap creates analysis difficulties (fit parameter correlations); however, some CP structure has moved to a higher energy near 3 eV. This is consistent with strain in the InAs, and there is no obvious physical reason why the $In_{0.53}Ga_{0.47}As$ CP should be shifted for these two samples.

For the AlAs samples, however, there is good reason to believe that the cap $In_{0.53}Ga_{0.47}As$ CPs might be shifted due to confinement by the AlAs which has much larger E_1 and $E_1+\Delta_1$ CP energies. The cap optical constants shown in Fig. 5 exhibit such a shift, which is larger for the thinner cap layer. The apparent increase in broadening may be accounted for by the greater importance of the rough oxide–cap interface for thinner layers. The strained AlAs optical constants for the thin group (Fig. 6) have no distinct E_1 CP structure; we believe this is due to a thin barrier effect as described previously. The optical constants for the thicker (~50 Å) AlAs layers exhibit a more pronounced peak at 4 eV and a shoulder just below 3.5 eV. Even though these layers are above the critical thickness and partially relaxed, our interpretation is that these layers still contain strong residual strain and that these two features are the strain-shifted E_1 and $E_1+\Delta_1$ CPs. We believe these structures are more visible in the thicker AlAs because the thin-barrier broadening effect has been reduced and optically there is more material to probe. The experimental shifts given in Table VII are for the thicker AlAs optical constants. The same basic agreement between calculation and experiment is seen for AlAs as was seen for the InAs. For AlAs the E_1 CP shifts the larger amount while the $E_1+\Delta_1$ CP is relatively stationary. It is tempting to look at Fig. 6 and also quantify a shift in the Γ-point band gap; however, below 3.2 eV, the AlAs optical constants begin to include a ''bleed through'' of imperfections from the cap optical constants and imperfect modeling of data oscillations due to the buffer layer. Thus, precise determination of the band gap is not possible. The strain model does predict, however, a fairly large shift to lower energies for the heavy-hole band gap.

To further illustrate that the washing out of the CP structure for the strained AlAs is not just a strain effect, another sample with the nominal structure of GaAs/AlAs/GaAs (20 Å/20 Å/substrate) was measured and analyzed with results shown in Fig. 10. (These measurements were also presented in Ref. 13.) The fitting models shown were identical except for the AlAs optical constants used. In both cases the oxide

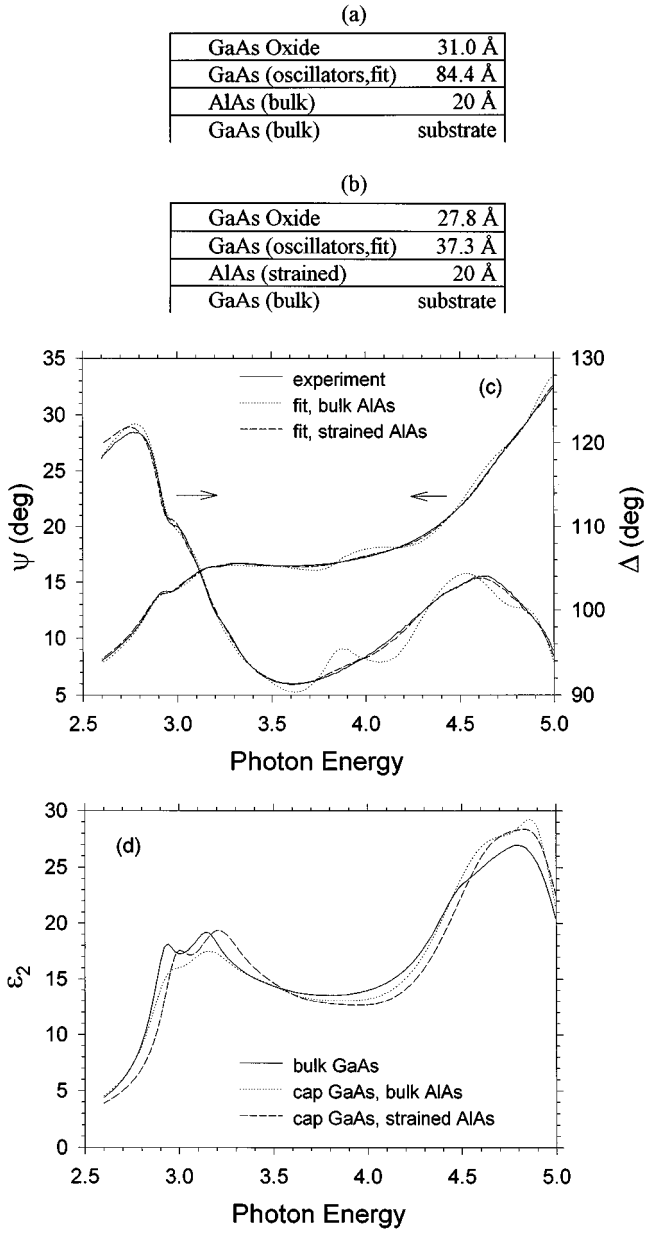

FIG. 10. Layered structures and fitted thicknesses used for modeling a sample with a thin (~20 Å) AlAs capped by nominally 20 Å of GaAs on a GaAs substrate. Each model had the same structure and fitting parameters, except that bulk AlAs optical constants were used in the first case (a), and strained AlAs optical constants were used in the second (b). (c) Experimental data and modeled data curves. (d) The resulting fitted GaAs cap optical constants.

thickness, cap thickness, and oscillator parameters for the cap optical constants were fit. The cap oscillator parameters were started, in both cases, as a good fit to bulk GaAs and only the broadening and energy parameters were allowed to vary. The resulting layered models, data fits, and cap optical constants are shown in Figs. 10(a)–10(d). When bulk AlAs values were used, noticeable AlAs CP features remained in the model [Fig. 10(c), 3.8 eV]. This procedure produced a poor fit with a very thick cap and lowered cap E_1 CP amplitudes [Fig. 10(d)]. The very large fitted cap thickness represented the minimization algorithm's attempt to reduce the importance of the AlAs features while maintaining the

proper model amplitudes in the GaAs E_1 region. A much better fit was obtained using the thin strained AlAs optical constants shown in Fig. 6. The resulting thicknesses [Fig. 10(b)] and cap optical constants [Fig. 10(d)] are much more reasonable (note that the cap E_1 features are blue shifted, while retaining their bulk amplitudes) even though the AlAs has very little strain (AlAs is almost lattice matched to GaAs). This is strong evidence that the thin-barrier (CP broadening) and strain (CP shifts, splitting) effects are distinct, and that the thin-barrier effect may be dominant for some material combinations.

The AlSb results closely mirror the AlAs results in the primary observation that the E_1 and $E_1+\Delta_1$ CP structures are washed out (Fig. 9). Also, the InAs cap (unstrained for the AlSb samples) optical constants exhibit a blue shift of their E_1 CP energies (Fig. 8). The major difference is that the E_2 CP structure for the InAs cap seems to also be washed out. This, however, can be accounted for by observing that the E_2 energy for AlSb is lower than that for InAs. Thus, while the InAs cap experiences a confinement of the E_1 wave functions, it behaves more barrierlike for the E_2 wave functions which are coupled to the corresponding lower-energy states in the AlSb. The constraints of oscillator modeled caps and the unknown thin AlSb optical constants make a unique fit in the E_2 region impossible. The apparent shift of the AlSb E_2 structure to 4.4 eV (Fig. 9) may not be totally correct for that reason. However, whatever ambiguities may exist in the E_2 region, the absence of CP structure around 3.2 eV in the data (Fig. 7) strongly confirms that the $E_1+\Delta_1$ CP is totally washed out for these strained AlSb layers.

VI. IMPLICATIONS FOR *IN SITU* GROWTH CONTROL

Controlling molecular-beam-epitaxy (MBE) growth using real-time spectroscopic ellipsometry requires the ability to fit parameters (typically thicknesses) of a dynamic model to the incoming data, and these fitted layer thicknesses are only meaningful if good fits are obtained. Even carefully obtained thin layer optical constants may not be sufficient when multiple layers are involved and quantum-mechanical effects become significant. During growth, the appropriate optical constants for previously grown layers may change as new layers are deposited. However, at high growth temperatures the CP structures (those not already washed out due to layer thinness) will be broadened. A spectroscopic control scheme can be made more sensitive to amplitudes away from the CPs and thus can be made less sensitive to subtle effects such as energy shifts in cap layers or quantum wells. (A single wavelength operating near an E_1 CP might be quite sensitive to quantum effects.) By passively examining many sample growths and correlating the real-time ellipsometric optical data with the electrical characterization of the devices, it should be possible to determine appropriate optical constants for thickness control. This might include changing optical constants in the model for buried layers before each new layer is grown. Any ellipsometric control scheme for thin layers will likely be complicated to set up, but this technique can provide some true feedback about what is actually being deposited on the sample surface over the widest range of sample conditions.

VII. CONCLUSIONS

Multi-sample analyses of spectroscopic ellipsometric data can be used to determine apparent optical constants for single, thin strained layers. For such samples, three principle effects have been identified as responsible for the change in optical constants away from their bulk values: strain, quantum confinement, and thin-barrier critical point broadening. Of the three, the thin-barrier effect is the newest and most pronounced. Optical constants for thin strained AlAs have also been shown to be compatible with data for thin unstrained AlAs layers on GaAs, thus demonstrating that the barrier broadening effect is not strain induced. The interplay of thin layer optical constants with their surroundings has definite implications for *in situ* growth control of thin, strained, and unstrained, layers. The sensitivity of dynamic ellipsometric measurements to growing samples is already well established, but the practicality of ellipsometric based thickness control schemes are based on the ability to extract meaningful, quantitative parameters. This *ex situ* work has neither proved nor disproved that *in situ* growth control of thin strained layers is possible, but it has demonstrated some optical effects which will be important and the need for spectroscopic measurements to account for them.

ACKNOWLEDGMENT

This work was supported by ARPA consortium Agreement No. MDA972-93-H-005.

[1] T. P. E. Broeckaert, W. Lee, and C. G. Fonstad, Appl. Phys. Lett. **53**, 1545 (1988).
[2] E. R. Brown, C. D. Parker, A. R. Calawa, M. J. Manfra, T. C. L. G. Sollner, C. L. Chen, S. W. Pang, and K. M. Molvar, Proc. SPIE **1288**, 122 (1990).
[3] E. R. Brown, S. J. Eglash, G. W. Turner, C. D. Parker, J. V. Pantano, and D. R. Calawa, IEEE Trans. Electron. Devices **ED-41**, 879 (1994).
[4] D. E. Aspnes, in *Handbook of Optical Constants of Solids*, edited by E. Palik (Academic, Orlando, 1985), Chap. 5.
[5] D. E. Aspnes, Thin Solid Films **233**, 1 (1990).
[6] D. E. Aspnes, W. E. Quinn, M. C. Tamargo, M. A. A. Pudensi, S. A. Schwarz, M. J. S. P. Brasil, R. E. Nahory, and S. Gregory, Appl. Phys. Lett. **60**, 1244 (1992).
[7] R. M. A. Azzam and N. M. Bashara, *Ellipsometry and Polarized Light* (North-Holland, New York, 1977), Chap. 4.
[8] C. M. Herzinger, P. G. Snyder, B. Johs, and J. A. Woollam, J. Appl. Phys. **77**, 1715 (1995).
[9] W. H. Press, B. P. Flannery, S. A. Teukolsky, and W. T. Vetterling, *Numerical Recipes: The Art of Scientific Computing* (Cambridge University Press, Cambridge, MA, 1988), Chap. 14.
[10] G. E. Jellison, Jr., Appl. Opt. **30**, 3354 (1991).
[11] S. Zollner, Appl. Phys. Lett. **63**, 2523 (1993).
[12] W. A. McGahan, B. Johs, and J. A. Woollam, Thin Solid Films **234**, 443 (1993).
[13] C. M. Herzinger, H. Yao, P. G. Snyder, F. G. Celii, Y.-C. Kao, B. Johs, and J. A. Woollam, J. Appl. Phys. **77**, 4677 (1995).
[14] M. Erman, J. B. Theeten, P. Chambon, S. M. Kelso, and D. E. Aspnes, J. Appl. Phys. **56**, 2664 (1984).
[15] H. D. Yao, P. G. Snyder, and J. A. Woollam, J. Appl. Phys. **70**, 3261 (1991).
[16] F. Terry, Jr., J. Appl. Phys. **70**, 409 (1991).
[17] F. G. Celii, Y.-C. Kao, L. A. Files-Sesler, E. A. Beam III, and H. Y. Liu (unpublished).
[18] M. Erman, J. B. Theeten, P. Frijlink, S. Gaillard, F. J. Hia, and C. Alibert, J. Appl. Phys. **56**, 3241 (1984).
[19] R. P. Vasquez, R. T. Kuroda, and A. Madhukar, J. Appl. Phys. **61**, 2973 (1987).

[20] J. C. Phillips, in *Solid State Physics*, edited by F. Seitz and D. Turnbull (Academic, New York, 1966), Vol. 18, p. 128.
[21] M. Chandrasekhar and F. H. Pollak, Phys. Rev. B **15**, 2127 (1977).
[22] V. Swaminathan, in *Indium Phosphide and Related Materials: Processing, Technology, and Devices*, edited by A. Katz (Artech House, Zürich, 1992), Chap. 1.
[23] F. H. Pollak, in *Strained-Layer Superlattices: Physics, Semiconductors and Semimetals*, edited by T. P. Pearsall (Academic, New York, 1990), Vol. 32, p. 40.
[24] *Semiconductors: Group IV Elements and III–V Compounds, Data in Science and Technology*, Vol. 1 (Springer, Berlin, 1991).
[25] C. Pickering, R. T. Carline, M. T. Emeny, N. S. Garawal, and L. K. Howard, Appl. Phys. Lett. **60**, 2412 (1992).
[26] C. Pickering, R. T. Carline, D. J. Robbins, W. Y. Leong, S. J. Barnett, A. D. Pitt, and A. G. Cullis, J. Appl. Phys. **73**, 239 (1993).
[27] R. T. Carline, C. Pickering, D. J. Robbins, W. Y. Leong, A. D. Pitt, and A. G. Cullis, Appl. Phys. Lett. **64**, 1114 (1994).
[28] C. Pickering and R. T. Carline, J. Appl. Phys. **75**, 4642 (1994).
[29] F. Lukes and K. Ploog, Thin Solid Films **233**, 162 (1993).
[30] D. E. Aspnes, in *Handbook on Semiconductors*, edited by M. Balkanski (North-Holland, Amsterdam, 1980), Vol. 2, p. 109.